JCI insight

The HIV latency reversing agent HODHBt inhibits the phosphatases PTPN1 and PTPN2

J. Natalie Howard, … , R. Brad Jones, Alberto Bosque

JCI Insight. 2024. https://doi.org/10.1172/jci.insight.179680.

Research In-Press Preview AIDS/HIV

Graphical abstract

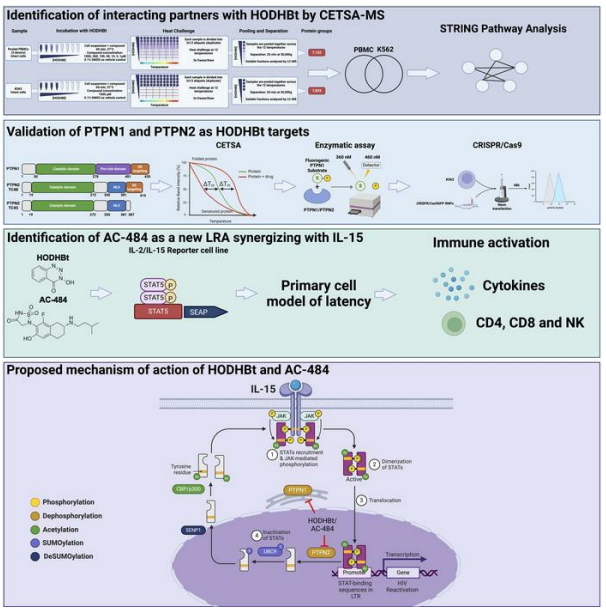

Find the latest version:

https://jci.me/179680/pdf

The HIV latency reversing agent HODHBt inhibits the phosphatases PTPN1 and PTPN2

Authors: J. Natalie Howard[1], Thomas D. Zaikos[2], Callie Levinger[1], Esteban Rivera[1], Elyse K. McMahon[1], Carissa S. Holmberg[1], Joshua Terao[1], Marta Sanz[1], Dennis C. Copertino Jr. [1,3], Weisheng Wang[1], Natalia Soriano-Sarabia[1], R. Brad Jones[3], Alberto Bosque[1*]

Affiliations:

[1]Department of Microbiology, Immunology, and Tropical Medicine, George Washington University, Washington DC 20037, USA.

[2]Department of Pathology, Johns Hopkins Hospital, Baltimore, MD, USA.

[3]Department of Medicine, Weill Cornell Medical College, New York, NY, USA.

*Corresponding author. Email: abosque@gwu.edu

Abstract:

Nonreceptor tyrosine phosphatases (NTPs) play an important role regulating protein phosphorylation and have been proposed as attractive therapeutic targets for cancer and metabolic diseases. We have previously identified that 3-Hydroxy-1,2,3-benzotriazin-4(3H)-one (HODHBt) enhanced STAT activation upon cytokine stimulation leading to increased reactivation of latent HIV and effector functions of NK and CD8 T cells. Here, we demonstrated that HODHBt interacts with and inhibits the NTPs PTPN1 and PTPN2 through a mixed inhibition mechanism. We also confirmed that PTPN1 and PTPN2 specifically control the phosphorylation of different STATs. The small molecule ABBV-CLS-484 (AC-484) is an active site inhibitor of PTPN1 and PTPN2 currently in clinical trials for advanced solid tumors. We compared AC-484 and HODHBt and found similar effects on STAT5 and immune activation

albeit with different mechanisms of action leading to varying effects on latency reversal. Our studies provide the first specific evidence that enhancing STAT phosphorylation via inhibition of PTPN1 and PTPN2 is an effective tool against HIV.

Introduction

Despite the development and rapid advancement of antiretroviral therapy (ART) against Human Immunodeficiency virus (HIV) in the past three decades, there remains no functional cure. This is due to the presence of intact and inducible provirus that is integrated within infected cells and unseen by the immune system allowing for viral persistence despite ART (1-3). Efforts to identify small molecules that can reactivate (or shock) latent virus into active replication, allowing cells to be seen and eliminated by immune effector cells, remains at the forefront of research today.

We have previously described that the small molecule, 3-Hydroxy-1,2,3-benzotriazin-4(3H)-one (HODHBt), is able to enhance cytokine-mediated STAT signaling (4). We initially identified HODHBt via a screening for compounds that could reactivate latent HIV in a primary cell model of latency (5). Our previous studies demonstrated that HODHBt was able to increase cytokine-induced phosphorylated STAT5 (pSTAT5), leading to enhanced binding of pSTAT5 to the HIV long terminal repeat (LTR). This resulted in viral transcriptional activation and latency reversal in primary CD4 T cells (4). We then described that the structural analogue 1,2,3-Benzotriazine-4(3H)-one (HBt) lacks biological activity, indicating the importance of the 3-hydroxy group in the biological activity of these compounds. Furthermore, we demonstrated that HODHBt lacks acute toxicity in mice and does not promote global immune activation (6). In follow-up studies, we showed that HODHBt enhanced the ability of IL-15 to 1) promote IFN-γ and Granzyme B production in NK cells leading to increased cytotoxic activity against HIV-infected cells and cancer cell lines (7), and 2) enhance the cytotoxic activity of HIV-specific

CD8 T cells via increasing the expression Granzyme B in CD8T cells and MHC-I expression on target cells (8). However, the direct target(s) of HODHBt remain unknown.

Here, to identify HODHBt target candidates, we used thermal proteomic profiling (TPP) (9-11). The two top hits were the nonreceptor tyrosine phosphatases (NTPs) protein tyrosine phosphatase nonreceptor type 1 (PTPN1) and type 2 (PTPN2), known for their activity in the regulation of the STAT signaling pathway (12-15). Utilizing biochemical and functional assays, we determined that HODHBt is a mixed inhibitor of PTPN1 and PTPN2. Recently, a small molecule dual active site inhibitor of PTPN1 and PTPN2, ABBV-CLS-484 (AC-484, Osunprotafib), has been characterized as a potent immune activator of anti-tumor responses (16), and there is one clinical trial in progress determining the effects of AC-484 against advanced solid tumors (NCT04777994). In this work, we compared the anti-HIV functions of these two PTPN1/PTPN2 inhibitors, HODHBt and AC-484. We showed that HODHBt and AC-484 have similar effects on STAT5 phosphorylation, induction of STAT5 transcriptional activity, immune cell activation, but differ in their ability to reactivate latent HIV in primary cells. These results show that PTPN1 and PTPN2 can be targeted to reverse latency, broadening current approaches for HIV cure.

Results

HODHBt modulates the thermal stability of PTPN1 and PTPN2.

TPP couples the cellular thermal shift assay (CETSA) with quantitative mass spectrometry (MS) (9-11), allowing precise identification of proteins that bind to a small molecule by identifying changes in protein stabilization of thousands of proteins simultaneously upon heating. TPP was performed in alive peripheral blood mononuclear cells (PBMCs) form HIV-negative donors and the chronic myelogenous leukemia cell line K562 cells treated with HODHBt (11, 17, 18). By performing TPP in living cells as opposed to cell lysates, we ensure

that the targets are 1) present at their physiological levels; 2) with their posttranslational modifications; 3) in their subcellular compartments; and 4) interacting with other proteins in their native conformation. We reliably quantified changes in stabilization of 7,122 and 7,829 proteins in PBMCs and K562 cells respectively (Supplemental File 1). HODHBt only changed the thermal stability of 119 proteins in PBMCs and 173 proteins in K562 cells ($p<0.01$) (Supplemental File 2). Among those, only 12 proteins were shared between both cell types (Figure 1A, Supplemental Figure 1, Supplemental File 2). Next, STRING pathway analysis identified three proteins with known interactions with STAT5: PTPN1, PTPN2, and CRKL (Supplemental File 3). PTPN1 and PTPN2 are two NTPs that regulate STAT5 activation, with PTPN1 being the predominant phosphatase present in the endoplasmic reticulum (ER), and PTPN2 being present in both the ER and nucleus (19, 20). CRKL is a proto-oncogene adaptor protein which has been shown to directly interfere with STAT5-DNA binding (21). To validate the TPP, we measured changes induced by HODHBt in thermal stabilization of different proteins in primary CD4 T cell lysates (10). Confirming our TPP, HODHBt specifically induced changes in the thermal stability of PTPN1 and PTPN2 compared to the inactive analogue HBt (Figure 1B, Supplemental Figure 2). We could not confirm changes in the thermal stability of CRKL. As controls, we evaluated changes in the thermal stability of STAT5, the ribosomal protein RPL7A, or the housekeeping gene β-actin, which did not show changes in thermal stability in our TPP (Supplemental File 1). We did not observe changes in the thermal stability of these three proteins (Figure 1B). Additionally, we measured changes in the thermal stability of purified PTPN1 and PTPN2 catalytic domain proteins induced by HODHBt and HBt compared to a DMSO control. For PTPN1, we observed stabilization by both HODHBt and the inactive control HBt compared to DMSO, whereas for PTPN2, we observed destabilization with HODHBt but not HBt (Figure 1C). This data suggests that the inactive control HBt could also binds to PTPN1 but does not

have the downstream effects of HODHBt. Next, to confirm the role of PTPN1 and PTPN2 regulating STAT5 phosphorylation (22) (23), both NTPs were individually or simultaneously knocked out using CRISPR-Cas9 in K562. We confirmed that knocking out both PTPN1 and PTPN2 results in enhanced STAT5 phosphorylation, suggesting that both NTPs are equally important in STAT5 regulation (Supplemental Figure 3A-C). Additionally, we observed that treatment of K562 cells with HODHBt resulted in a dose-dependent increase in pSTAT5 concomitant with a reduction on the levels of PTPN2 and to a lesser extent of PTPN1 (Supplemental Figure 3D), suggesting that HODHBt may promote changes in the expression of these two phosphatases.

HODHBt is a mixed inhibitor of PTPN1 and PTPN2.

PTPN1 and PTPN2 belong to the Class I PTP family and share an overall 72% sequence similarity overall and 94% similarity for the catalytic domain, including the cysteine residue required for full enzymatic function (24, 25) (Supplemental Figure 4). Using recombinant PTPs in vitro, we characterized HODHBt's mechanism of inhibition. HODHBt inhibited the catalytic activities of both PTPN1 and PTPN2 compared to the inactive structural analogue HBt with average IC50s of 601μM and 544μM, respectively (Figure 2A). To determine the mechanism of inhibition, we performed a kinetic analysis using varying concentrations of both the substrate and HODHBt (Figure 2B). This allowed us to perform Michaelis-Menten least square fit analysis to determine the Vmax and Km for each HODHBt concentration, where Vmax is the extrapolated maximum enzyme velocity and Km is the substrate concentration needed to achieve a half-maximum enzyme velocity (also known as the Michaelis-Menten constant) (Supplemental Figure 5). Using the calculated Vmax and Km values, we fitted the data to Lineweaver-Burk plots and determined that HODHBt is a mixed inhibitor. A mixed inhibitor is defined as an

inhibitor that can either bind to the enzyme at an allosteric site regardless of whether the substrate is bound or bind at an allosteric site to the already bound enzyme-substrate complex (26, 27). Both scenarios result in a decrease in the Vmax, but preferential binding of the inhibitor to free enzyme increases the Km, while binding to the enzyme-substrate complex decreases the Km (27). Our results suggest potential preferential binding of HODHBt to free PTPN1 and PTPN2-substrate complex based on the increased and decreased Km values respectively (Figure 2C, Supplemental Figure 5). Together, our results demonstrate that HODHBt binds and inhibits the catalytic domain of PTPN1 and PTPN2 and constitute a novel class of compounds that act as dual PTPN1/PTPN2 mixed inhibitors.

PTPN1 and PTPN2 control the phosphorylation and transcriptional activity of STATs in a cytokine-specific manner

We have reported previously that in addition to enhancing STAT5A and STAT5B phosphorylation, HODHBt also enhances the phosphorylation of STAT1 and STAT3 upon IL-15 stimulation (6, 7). To test whether inhibiting PTPN1 and PTPN2 with HODHBt enhanced phosphorylation of additional STATs, we isolated and treated primary total CD4s with four different cytokines targeting activation of one or more specific STATs for 24 hours (28). As previously reported, HODHBt alone did not significantly increase STAT phosphorylation (4). However, stimulation with IL-15 combined with HODHBt resulted in increased phosphorylation of STAT1, STAT3, STAT4, and STAT5 compared to the inactive control HBt. HODHBt also enhanced IFNα-mediated STAT1 phosphorylation but not STAT2 (Figure 3A, B). We confirmed that HODHBt does not enhance phosphorylation of STAT2 in both total CD4 T cells in the presence of IFN-α (Figure 3C), and in 293FT cells stably transfected with V2-tagged STAT2 (Figure 3D). Stimulation with IL-12 in the presence of HODHBt resulted in increased

phosphorylation of STAT1 while HODHBt did not influence IL-4-mediated STAT6 phosphorylation (Figure 3A, B). Failure of HODHBt to enhance STAT2 phosphorylation suggests that PTPN1 and PTPN2 might not control STAT2 transcriptional activity. STAT2, in combination with STAT1, are important for regulating interferon (IFN) signaling. While type-I IFNα/β requires STAT1 and STAT2 heterodimers and binding to interferon-sensitive response element (ISRE), type-II IFNγ signals through STAT1 homodimers and gamma interferon activation site (GAS) elements (29-31). Based on our previous work, we hypothesized that inhibiting PTPN1 and PTPN2 with HODHBt would enhance IFNγ but not IFNα/β. We confirmed that inhibiting PTPN1 and PTPN2 with HODHBt did not enhance IFNα or IFNβ activation of the ISRE promoter (Figure 3E). On the other hand, HODHBt enhanced IFNγ activation of the GAS promoter in a dose-dependent manner (Figure 3F). These data suggest that PTPN1 and PTPN2 regulate the phosphorylation of all STAT isoforms except STAT2 and STAT6. This could be attributed to the fact that both PTPN1 and PTPN2 preferentially bind to bi-phosphorylated substrates (32). All STATs, excluding STAT2 and STAT6, have a conserved serine residue that can be phosphorylated in addition to the ubiquitous C-terminal tyrosine residue required for SH2 partner interaction and dimerization (33). Overall, our findings confirm that PTPN1 and PTPN2 control the phosphorylation and transcriptional activity of STAT-1, 3, 4 and 5 and that HODHBt enhances STAT transcriptional activation in a cytokine-specific manner.

AC-484 promotes immune activation and synergizes with IL-15 to reactivate latent HIV

AC-484 is a newly characterized active site dual inhibitor of PTPN1 and PTPN2 with potent anti-tumor effects (16) that is currently in clinical trials for patients with advanced solid tumors (NCT04777994). We sought to investigate the potential of AC-484 as an HIV LRA compared to HODHBt. Structurally, HODHBt and AC-484 share a core benzene ring but lack

other substantial similarities that could explain their shared inhibition of PTPN1 and PTPN2 (Figure 4A). First, we evaluated the effects on STAT5 transcriptional activity using HEK-Blue-IL2/IL15 cells as previously described (6). Compared to HODHBt, AC-484 was about 100-fold more potent at increasing STAT5 transcriptional activity, with an EC50 of 7.25μM compared to 762μM of HODHBt (Figure 4B), and there was no observed toxicity with either compound (Figure 4C). These initial findings suggested that perhaps AC-484 would be able to reactivate latent HIV to a similar, if not greater degree, as HODHBt. Given the current clinical relevance of IL-15 as an LRA (34), we next investigated the LRA efficacy of combining HODHBt and AC-484 with IL-15. We observed that HODHBt alone has minimal LRA activity (8.2% of the maximal stimulus αCD3/28 beads) and observed similar minor significant levels with AC-484 (7.8%). Treatment with IL-15 induced higher frequency of HIV p24+ cells compared to the DMSO control (27.1% vs. 0%, Figure 4D). Additionally, the combination of HODHBt and IL-15 led to significant reactivation compared to DMSO (54.4% vs. 0%, p=0.003, Figure 4D) and synergistic viral reactivation compared to IL-15 alone (Figure 4E). AC-484 with IL-15 also resulted in significantly higher reactivation than the DMSO control (42.3% vs. 0%, p=0.03), and was synergistic with IL-15, albeit to a lesser degree than HODHBt (Figure 4D, E). Similar results were observed with IL-2 albeit the degree of reactivation was lower than with IL-15 (Supplemental Figure 6). These results show that AC-484 can enhance the LRA activity of IL-15.

We have previously shown that HODHBt in the absence of exogenous cytokine is sufficient to induce immune activation of multiple cell subsets in PBMCs from HIV-negative individuals and aviremic people living with HIV (PWH) (6). AC-484 has also been shown to increase CD69 expression on T cells in whole blood in a dose-dependent manner (16). To investigate whether AC-484 induces immune activation of CD4, CD8, and NK cells, we

191 performed dose response experiments of AC-484 in PBMCs with and without low dose IL-15
192 and compared the effects to HODHBt. We used AC-484 concentrations from 500nM to 10μM
193 and compared to 100μM HODHBt alone and in the presence of 1ng/ml of IL-15. In the absence
194 of cytokine, AC-484 induced the expression of CD69 in CD4T, CD8T and NK cells in a dose-
195 dependent manner reaching similar levels as 100μM HODHBt at the highest concentration tested
196 (10μM) (Figure 4F). Similar results were observed in the presence of IL-15 but the magnitude of
197 the response was increased compared to no cytokine treatment. Next, we sought to further
198 investigate the effects of AC-484 on immune activation and production of pro-inflammatory
199 cytokines, a potentially unwanted consequence of manipulating STAT signaling for HIV cure
200 approaches. We have previously shown that HODHBt does not promote the secretion of pro-
201 inflammatory cytokines (4). On the other hand, AC-484 has been shown to trigger production of
202 the pro-inflammatory cytokines IFNγ and TNFα in mouse T cells (16). Using a 10-plex cytokine
203 ELISA, we saw no significant increase after treatment with HODHBt or any of the AC-484
204 concentrations alone or with IL-15 of different pro- and anti-inflammatory cytokines (Figure
205 4G). This data shows that AC-484 is sufficient to induce immune activation in various cell
206 subsets without inducing a pro-inflammatory cytokine profile.
207
208 ***Effects of HODHBt and AC-484 on STAT5 activity***
209 Although AC-484 was a more potent STAT5 activator in the HEK-Blue-IL2/IL15 cells, it
210 had lower activity than HODHBt reactivating latent HIV in a primary cell model of HIV latency.
211 We have previously shown that HODHBt maintains prolong STAT5 activation upon cytokine
212 signaling, leading to increased nuclear presence (4). We then performed a pSTAT5 time course
213 experiment in primary total CD4 T cells with and without IL-2. After 1 hour and 24 hours in the
214 presence of IL-2, HODHBT and AC-484 induced higher pSTAT5 compared to IL-2 alone. As

expected, HODHBt sustained IL-2 mediated pSTAT5 up to 48 hours (Figure 5A). On the other hand, AC-484 was unable to maintain levels of pSTAT5 over IL-2 treatment alone, but this reduction on pSTAT5 levels was not associated with toxicity (Supplemental Figure 7A). Similar results were observed with IL-15 (Figure 5B) without an effect on viability (Supplemental Figure 7B). We have shown that HODHBt is able to reduce the levels of PTPN1 and PTPN2 in K562 cells (Supplemental Figure 3D), potentially explaining the persistent pSTAT5 over time. We then analyzed whether AC-484 was able to reduce PTPN1 and PTPN2 levels. We evaluated changes in both NTP levels after treatment with either HODHBt or AC-484 +/- IL-2 in primary CD4 T cells for 24 hours. In the absence of cytokine, we observed no significant changes in the levels of either PTPN1 or PTPN2 levels after treatment with HODHBt or AC-484 compared to DMSO. However, in the presence of IL-2, we observed a decrease, albeit not significant, in the levels of both PTPN1 and PTPN2 after treatment with HODHBt but not AC-484 compared with IL-2 alone. As expected, we observed a significant increase in pSTAT5 levels after treatment with IL-2 and HODHBt and to a lesser extent with IL-2 and AC-484 compared to IL-2 alone (Figure 5C), confirming the flow cytometry analysis (Figure 5A). In the presence of IL-15, HODHBt treatment similarly resulted in significantly increased pSTAT5 levels and decreased PTPN2 levels, whereas AC-484 again did not enhance pSTAT5 levels or significantly changed the levels of PTPN1 and PTPN2 over IL-15 alone (Figure 5D). Together, this data shows that AC-484 is not able to sustain pSTAT5 levels over time to the same degree as HODHBt either alone or in the presence of γc-cytokines. A potential difference between both compounds that could explain these results is the lack of ability of AC-484 to alter the levels of PTPN1 and PTPN2 compared with HODHBt.

Discussion:

In this work, we have characterized HODHBt as a PTPN1/PTPN2 inhibitor that directly interacts with PTPN1 and PTPN2, inducing changes in the thermal stability of both proteins in vitro, and leading to enhanced phosphorylation and transcriptional activation of different STATs. Because of the relevance of our previous work showing that HODHBt enhances immune functions and latency reversal, we analyzed the functions of the recently developed and clinically relevant PTPN1/PTPN2 active site inhibitor AC-484. Our results demonstrated that like HODHBt, AC-484 promotes STAT5 transcriptional activation, induces immune activation, and synergizes with IL-15 to reactivate latency in an in vitro primary cell model of latency, albeit with a different mechanism of action.

In the context of HIV, we have previously shown that HODHBt increases cytokine-mediated HIV reactivation from latency due to enhanced STAT5 transcriptional activation and binding to the HIV LTR (4). In addition, we have demonstrated that HODHBt reactivates latent virus in cells isolated from ART-suppressed PLWH (6), and can also enhance NK cell killing of HIV-infected cells through increased STAT activation upon IL-15 treatment (7). Our identification of PTPN1 and PTPN2 as the targets of HODHBt is important and very relevant given the growing body of literature highlighting both NTPs as attractive therapeutic targets for cancer (22, 23, 35-38); and metabolic diseases such as diabetes and obesity (39-42). We have previously shown that HODHBt enhanced STAT5 phosphorylation and this led to a reduction on STAT5 SUMOylation and accumulation in the nucleus in primary CD4T cells (4). At the time, we did not know the actual targets of HODHBt. Based on our current and past studies, we now proposed that HODHBt and AC-484 target PTPN1 and PTPN2 and suggest that dephosphorylation is a step required for SUMOylation of STAT5 and translocation back into the cytoplasm (Figure 6) (4).

A recent study investigating a related compound of AC-484, Compound-182, exhibited promise in small animal models for cancer therapeutics by demonstrating that in vivo administration of Compound-182 led to augmented activation and recruitment of T cells in solid tumors, resulting in a reduction in tumor growth (43). Crucially, this was achieved without triggering the development of cytokine release syndrome or autoimmunity, suggesting that targeting PTPN1 and PTPN2 in vivo may not be associated with toxicities caused by immune system over-activation. Our work demonstrates that these targets can now be expanded to other infectious diseases and in particular, to HIV.

The ability of AC-484 to enhance immune activation and STAT5 phosphorylation through inhibition of PTPN1 and PTPN2 (16) led us to hypothesize that AC-484 functions similarly to HODHBt and has the potential for use as a component of HIV cure strategies. Direct comparison of HODHBt and AC-484 on STAT5 transcriptional activity with and without IL-15 showed that AC-484 is a much more potent transcriptional activator in the HEK-Blue-IL2/IL15 cell line. However, we saw lower activity of AC-484 in reversing HIV latency. We speculate that the differences on transcriptional activation seen between HODHBt and AC-484 are cell type and/or gene-dependent. The HEK-Blue-IL2/IL15 cell line has been optimized so that STAT5 binding is the only signal needed to induce transcriptional activation. The HIV LTR is a complex promoter subject to epigenetic regulation such as histone acetylation and histone methylation among others (44-47). Furthermore, in primary CD4 T cells, effective latency reversal must overcome several blocks, including blocks in elongation, splicing, nuclear export and/or translation (48-53). We have demonstrated that one of the key effects of HODHBt is sustained γc-cytokine-stimulated STAT5 phosphorylation over time which may facilitate increased HIV latency reversal (4). In primary total CD4 T cells, we observed that AC-484 failed to promote sustained STAT5 phosphorylation overtime. We hypothesize that the inability of AC-484 to

sustain STAT5 phosphorylation is why we did not see greater latency reversal in the primary cell model compared to HODHBt. Mechanistically, we observe that HODHBt led to a reduction on the levels of PTPN1 and PTPN2, which it was not observed with AC-484. Our previous studies with HODHBt, did not observe changes in the transcription of either phosphatase (4), suggesting that another mechanism such as proteasomal or lysosomal degradation may be involved in this process. Further studies will be warranted to elucidate the exact mechanism by which HODHBt reduces the protein levels of PTPN2 and to a lesser extent PTPN1. Despite these differences between HODHBt and AC-484, we confirmed that both compounds can synergize with IL-15 to reactivate latent HIV, are sufficient to induce immune activation of CD4, CD8 T and NK cells, but AC-484 had activity at a 10-fold less concentration compared to HODHBt. Additionally, neither compounds induce production of pro-inflammatory cytokines in PBMCs which is an important factor when developing new HIV LRAs.

Given our findings that AC-484 is sufficient to promote immune activation despite reduced latency reversal activity compared with HODHBt, future directions for this work will investigate the effects of AC-484 on the anti-HIV activity of immune effector cells including CD8 T cells and NK cells and its latency reversal properties in combination with other LRAs. Overall, our work highlights the possible therapeutic potential of PTPN1 and PTPN2 inhibition, leading to enhanced STAT activity, in the search for globally applicable and achievable HIV cure strategies.

Materials and Methods:

CETSA-MS

CETSA-MS was performed at Pelago Biosciences, Sweden.

Sample Matrix

Pooled Human Peripheral Blood Mononuclear Cells (PBMCs) were purchased from 3H Biomedical (Sweden). Cells where thawed the day before the experiment in RPMI 1640 medium supplemented with 10% FBS and 1% pen/strep (all from Gibco) and cultured at 37°C and 5% CO_2. For the experiment, the cells were pelleted, washed with Hank's Balanced Salt solution (HBSS, Thermo Fisher Scientific), and pelleted again. Cell viability was measured with trypan blue exclusion and cells with a viability above 90% were used for the experiment.

K562 cells were obtained from ATCC (CCL-243). They were cultured at 37°C and 5% CO_2 in RPMI 1640 medium with 10% FBS and 1% pen/strep (all from Gibco). For the experiment, the cells were pelleted, washed with Hank's Balanced Salt solution (HBSS, Thermo Fisher Scientific), and pelleted again. Cell viability was measured with trypan blue exclusion and cells with a viability above 90% were used for the experiment.

For both cell types, cell pellets were resuspended in CETSA buffer (20mM HEPES, 138mM NaCl, 1mM $MgCl_2$, 5mM KCl, 2mM $CaCl_2$, pH 7.4) at a density of $40*10^6$cells/mL and used as the 2x matrix solution.

Compounds

HODHBt was purchased from Bio-techne (# 6994) and stored at -20°C.

Compressed CETSA-MS experiment

PBMCs were divided into eight aliquots each and mixed with an equal volume of either one of the seven test compound concentrations or control at 2x final concentration in the experimental buffer. The resulting final concentrations of the compound were 1, 3, 10, 30, 100, 300 and 1000 µM; 0.1% DMSO was used as a vehicle control. For K562, 1000µM of HODHBt or 0.1% DMSO were done in quadruplicates. Incubations were performed for 60 minutes at 37°C.

Each of the eight treated samples (8 concentration points) was divided into 24 aliquots (12 temperature points, two replicates) that were all subjected to a heat challenge. After heating, all

temperature points for each test condition were pooled to generate 8 x 2 individual (compressed) samples. In addition, non- heated samples were processed alongside the experiment in a single replicate and used to distinguish between changes in thermal stability and changes in protein abundance caused by the treatment.

Precipitated proteins were pelleted by centrifugation and supernatants constituting the soluble protein fraction were kept for further analysis.

Protein digestion and labeling

Equal amounts of total protein from each soluble fraction were subjected to reduction and denaturation, followed by alkylation with chloroacetamide. Proteins were subsequently digested with Lys-C and trypsin.

After complete digestion had been confirmed by nanoLC-MS/MS, samples were labelled with 16-plex Tandem Mass Tag reagents (TMTPro, Thermo Scientific) according to the manufacturer's protocol.

LC-MS/MS analysis

For each TMT16-plex set, peptides were separated by multidimensional chromatography, and high- resolution MS/MS data was acquired with a Orbitrap Exploris 240 mass spectrometer coupled to a Dionex Ultimate3000 nanoLC system (both from Thermo Scientific).

Protein identification and quantification

Protein identification was performed by database search against 95, 607 human protein sequences in Uniprot (UP000005640, download date: 2019-02-21) using the Sequest HT algorithm as implemented in the ProteomeDiscoverer 2.5 software package. Data was re-calibrated using the recalibration function in PD2.5 and final search tolerance setting included a mass accuracy of 10 ppm and 50 mDa for precursor and fragment ions, respectively. A maximum of 2 missed cleavage sites was allowed using fully tryptic cleavage enzyme specificity

(K, R, no P). Dynamic modifications were oxidation of Methionine, and deamidation of Asparagine and Glutamine. Dynamic modification of protein N-termini by acetylation was also allowed. Carbamidomethylation of Cysteine, TMTPro-modification of Lysine and peptide N-termini were set as static modifications.

For protein identification, validation was done at the peptide-spectrum-match (PSM) level using the following acceptance criteria; 1 % FDR determined by Percolator scoring based on Q-value, rank 1 peptide only.

For quantification, a maximum co-isolation of 50 % was allowed. Reporter ion integration was done at 20 ppm tolerance and the integration result was verified by manual inspection to ensure the tolerance setting was applicable. For individual spectra, an average reporter ion signal-to-noise of >20 was required. Further, shared peptide sequences were not used for quantification.

Compressed CETSA MS data processing and ranking

Protein intensities were normalized ensuring same total ion current in each quantification channel. Intensity values were then $\log_2$-transformed and aligned between treatments and replicates, so as each protein has the same mean intensity in all treatments and replicates.

The fold-changes of any given protein across the concentration range is quantified by using the vehicle condition as the reference (i.e., a constant value of 1). Fold-changes are also transformed to $\log_2$ values, to achieve a normal distribution around 0. Processed data is uploaded to Pelago's data portal.

To estimate effect size (amplitude) and p-value (significance) of the protein hits, the individual protein concentration-response curve is fitted using the following formula:

$$logI \sim A + \frac{B - A}{1 + e^{\frac{C_M - C}{scale}}}$$

were $logI$ — $\log_2$-transformed protein intensity, C — $\log_{10}$-transformed compound concentration, A, B, C_M and $scale$ — curve parameters for the fit. Using the values from the model fit, the effective concentration corresponding to 50% of maximal signal is estimated: $pEC_M* = -C_M$. Apparent pEC_M* values should be used with caution, given the short incubation time and the specific experiment design.

Significance of the effect for each protein is assessed using ANOVA F-test using the model fitted with formula above. Benjamini-Hochberg correction is applied to F-test derived p-values to adjust for multiple comparison.

Reagents

Human recombinant interleukin-2 (rIL-2) and recombinant interleukin-15 (rIL-15) were obtained via the BRB/NCI Preclinical Repository. Human αIL-12 (500-P154G), αIL-4 (500-P24), TGF-β (100–21), rIL12 (200-12), rIL-4 (200-04), rIL-21 (200-21), rIL-7 (200-07), and rhIFN-β (300-02BC) were purchased from Peprotech. Human rIFN-α2 (NBP2-34971) was purchased from Novus Biologicals. Human rIFN-γ (570206) was purchased from BioLegend. Raltegravir (#HRP-11680) and Nelfinavir (#ARP-4621) from NIH HIV Reagent Program. Fluorogenic PTP1B catalytic domain assay kit (#79764) and recombinant GST-tag TC-PTP (PTPN2, #30013) were purchased from BPSBioscience. CRISPR GFP-Cas9, PTPN1 and PTPN2 crRNA, and tracrRNA were purchased from IDT. ABBV-CLS-484 (HY-145923) was purchased from MedChem Express. HEK-Blue CLR selection cocktail (h-csm), Puromycin (ant-pr-1), Blasticidin (ant-bl-1), Zeocin (ant-zn-1), and QUANTI-Blue solution (rep-qbs2) purchased from Invivogen. CytoTox 96 non-radioactive cytotoxicity assay (#G1780) was purchased from Promega. CorPlex Cytokine panel kit was ordered from Quanterix (85-0329). Antibodies were purchased from BioLegend (PE αSTAT5 Phospho (Y694) #936903, FITC αCD4 #300506,

PerCPCy5.5 αCD56 #362506, APC-Cy7 αCD69 #310914), eBiosciences (eF450 fixable viability dye), BD Horizon (BV786 αCD3 #563918, Human FC block #564220), Thermo Fisher Scientific (PE αCD8 #12-0086-42), Beckman Coulter (FITC KC57 #6604665), Cell Signaling Technologies (PTP1B- #5311S, TC-PTP (TC45)- 58935S, CRKL- #38710S, STAT5- #94205S, RPL7A- #2415S, pSTAT5 (Y694)- #9359S, pSTAT1(Y701)- #7649S, STAT1- #9177S, pSTAT3 (Y705)- #9145S, STAT3- #9139S, pSTAT2- #4441P, STAT2- #4594S, pSTAT4- #4134S, STAT4- #2653S, pSTAT6- #9361S, STAT6- #9362S), Proteintech (PTPN2 polyclonal- 11214-1-AP), Sigma Aldrich (β-actin (AC-15)- #A5441), and Jackson ImmunoResearch (αRabbit 2° #111-035-046, αMouse 2° #115-0350146).

K562 cells were a gift from Katherine Chiappinelli (George Washington University, Washington DC).

Methods

Sex as a biological variable

All experiments using primary human peripheral blood mononuclear cells use cells isolated from both male and female donors.

Cell Line Culture

K562 were cultured in complete RPMI.

CETSA

For the CETSA experiments, the protocol was adapted from Jafari et al. Naïve CD4 T cells were isolated from donor peripheral blood mononuclear cells by negative selection and activated using αCD3/CD28 beads (Dynal/Invitrogen) for 72 hours as previously described (5). The cells were then expanded for a further 7 days in the presence of 30 IU/mL IL-2 in RPMI supplemented with 1% L-glutamine, 10% fetal bovine serum (FBS), and 1% penicillin-streptomycin (PS) (complete RPMI). On day 10, the cells were washed with PBS and resuspended in PBS supplemented with

protease inhibitor cocktail (cOmplete, Roche), and phosphatase inhibitor cocktail (phosSTOP, Roche) at a concentration of $20x10^6$ cells/mL. Cell suspensions were lysed by freeze-thaw three times in liquid nitrogen and the lysate fractions were separated from debris by centrifugation at 20,000g for 20 minutes at 4°C. Cell lysates were treated with 100μM HODHBt or the inactive control HBt and incubated at 25°C for 30 minutes. Samples were then separated into 7x50μL aliquots and heated at increasing temperatures for 3 minutes using a thermocycler. The samples were spun down at 15,000 rpm for 10 minutes to remove precipitates and analyzed by Western blot. The following antibodies were used at the noted concentrations: STAT5 (1:1000), pSTAT5 (1:1000), CRKL (1:1000), PTPN1 (1:500), PTPN2 (1:1000), and β-actin (1:5000). Band intensities were quantified and plotted as a function of temperature to generate the melting curves of each protein/treatment combination.

For the purified protein CETSAs, PTPN1 catalytic domain was purified as described below. TC-PTP (PTPN2) catalytic domain protein was purchased from BPS Bioscience (#30013). Protein was diluted to equal 62.5ng in 100μL PBS supplemented with protease and phosphatase inhibitors (described below). The protein dilutions were treated with DMSO, 100μM HODHBt or the inactive control HBt and incubated at 25°C for 30 minutes. Samples were then split into 2x50μL aliquots and heated at 55°C for 3 minutes using a thermocycler. The samples were spun down at 15,000 rpm for 10 minutes to remove precipitates and analyzed by Western blot. The following antibodies were used at the noted concentrations: PTPN1 (1:1000) and PTPN2 (Proteintech, 1:1000). Band intensities were quantified and plotted as a function of temperature compared to the unheated control.

<u>PTPN1 protein purification</u>

PTPN1 protein was kindly provided by Heidi Schubert and Chris Hill (University of Utah). 2L of His-TEV-PTP1B (catalytic domain: 1-301) (Addgene 102719) in BL21(DE3)RIL cells were

grown in Luria broth at 37C until they reached an OD600=0.6 and then cooled, induced to a final concentration of 0.4mM IPTG and grown overnight at 18C. The cell pellet was resuspended in 80mls of lysis buffer (20mM Tris pH 7.5, 40mM Imidazole, 300mM NaCl, 10% glycerol) with protease inhibitors leupeptin, aprotinin and pepstatin. The sample was sonicated prior to a high speed spin to pellet the insoluble fraction. The soluble supernatant was incubated with 5mls equilibrated Qiagen NiNTA resin for 30" prior to washing the resin with an additional 100mls of lysis buffer. The salt concentration was reduced to 100mM prior to elution (20mM Tris pH 7.5, 250 mM Imidazole, 100 mM NaCl, 10% glycerol). The protein was dialyzed against 50mM Tris pH 8.0. 500 mM NaCl, 1mM DTT and homemade TEV protease was added overnight. A s200 SEC column was run in 20mM Tris pH 7.5, 50mM NaCl, 1mM DTT to finish the preparation. The protein was concentrated to 7-9mgml and stored at -80.

PTPN1/PTPN2 Catalytic Domain Inhibition Assay

HODHBt inhibition (IC_{50}) of PTPN1 enzymatic activity was measured using the fluorogenic PTP1B (catalytic domain) assay kit (BPS Bioscience, #79764) following manufacturer's instructions. It is designed to measure inhibition of enzyme catalyzation of dephosphorylation of fluorogenic substrate. For PTPN2, the catalytic domain of TC-PTP (PTPN2) was used instead of PTP1B (PTPN1).

The mode of inhibition of HODHBt was determined by adding a final concentration of 0.4 pg/mL of each enzyme to varying concentrations of PTP substrate and HODHBt. The fluorescence signal was measured every 15 seconds for 30 minutes by spectrophotometer using an excitation wavelength of 360 nm and an emission wavelength of 460 nm. Data was analyzed using GraphPad 9.0 software and Michaelis-Mention equation fit.

Genome Editing via CRISPR/Cas9

Pre-designed guide RNAs for PTPN1 (ACCACAACGGGCCCGTGCTC) and PTPN2 (GCACTACAGTGGATCACCGC) were obtained from IDT. Protocol for transfection by electroporation with the Neon from IDT was followed. Briefly, RNPs for PTPN1 and PTPN2 were prepared by first incubating 200μM Alt-R-CRISPR-Cas9 crRNA (IDT) and Alt-R-CRISPR-Cas9 tracrRNA (IDT) (final duplex concentration of 44μM) at 95°C for 5 minutes. The guide RNA duplexes were then combined with Alt-R Cas9 GFP (final concentrations 22pmol and 18pmol respectively) and incubated at room temperature for 10-20 minutes as per the manufacturer's instructions. The RNPs were then transfected into K562 cells ($0.25x10^6$ per reaction) by electroporation. For the PTPN1+PTPN2 dual condition, equal volumes of PTPN1 and PTPN2 RNP were transfected into the cells via electroporation (Neon). 48 hours later, $0.5x10^6$ K562 cells were collected and stained for phospho-STAT5. The rest were collected for gDNA isolation and knockout efficiency determination (described below).

Knockout Efficiency Analysis of CRISPR/Cas9-edited K562 cells:

Genomic DNA (gDNA) was obtained from cell pellets by resuspending in 50μL Quick Extract DNA Extraction Solution (Lucigen, #QE0905T) and following the extraction program as per the manufacturer's instructions. Genomic DNA (2μL) was then PCR amplified (50μL total reaction volume) using the following primers: PTPN1 Forward (5'-CTATACCACATGGCCTGACTTT-3'), PTPN1 Reverse (5'-GAGTCTCAGGTACGCCTTTATTAG-3'), PTPN2 Forward (5'-ACTGCCAGTGGAAGCAAT-3'), PTPN2 Reverse (5'-TTTGGAGTCCCTGAATCACC-3'). Knockout efficiency was measured using the T7endonuclease I from NEB (#M0302S) and following manufacturer's instructions. Analysis was performed using the GelAnalyzer 19.1 software and T7EI beta tool from Horizon Discovery.

Primary cell model of latency:

Naïve CD4+ T cells were isolated via negative selection from PBMCs obtained from HIV negative donors. Cultured T_{CM} were generated and infected as previously described (5, 54, 55). Naïve CD4 T cells were isolated from PBMCs from HIV-negative donors by negative selection (Stemcell #19555) and activated at $0.5x10^6$ cells/mL with αCD3/CD28 Dynabeads (1:1 bead-to-cell ratio) in the presence of 1μg/mL αIL-4, 2μg/mL αIL-12, and 10ng/mL TGF-β for 72 hours. Dynabeads were removed on day 3 and cells were subsequently expanded in RPMI supplemented with 1% L-Glutamine, 10% Fetal Bovine Serum, and 1% penicillin/streptomycin (complete RPMI) with 30 IU/ml IL-2 before being infected on day 7 via spinoculation with the X4-tropic virus NL4-3. Levels of intracellular p24 were assessed 72 hours later (day 10) by flow cytometry prior to the infected cells being crowded in 96-well round bottom plates to facilitate spread of infection (100,000 cells/well). On day 13, the cells were uncrowded and plated in the presence of an ART cocktail (1μM Raltegravir + 0.5μM Nelfinavir) and 30IU/ml IL-2, and p24 levels were again measured by flow cytometry. 96 hours later (day 17), the CD4 positive cells were sorted from the infected cultures by positive selection (Dynabeads CD4 positive Isolation kit, Thermo Fisher Scientific #11331D), and p24 levels were measured pre- and post- sort. The CD4 positive cells were then resuspended at $1x10^6$ cells/mL and plated with reactivation conditions for a further 48 hours and reactivation was measured by p24 stain on day 19.

Flow cytometry:

Flow cytometry was used to measure the levels of STAT5 phosphorylation in the CRISPR/Cas9-edited K562 cells and total CD4+ T cells, as well as immune activation in PBMCs. Between 0.3-$0.5x10^6$ cells for each condition were collected and washed with PBS before resuspension in 100μL FACS buffer (PBS+2% FBS) with 0.1μL viability dye (eBioscience Fixable Viability Dye eFluor 450, Thermo Fisher Scientific cat#: 65-0863-18). For immune activation flow cytometry, PBMCs were incubated with Fc block (564220, BD Biosciences) prior to staining

with viability dye. Cells were incubated for 10min at 4°C before being washed with 500µL FACS buffer. Cells were then resuspended in 100µL pre-warmed Fix Buffer I (BD Bioscience cat#:557870) and incubated at 37°C for 10 minutes. Cells were washed with 500µL FACS buffer, resuspended in pre-cooled Perm Buffer III (BD Bioscience cat#:558050), and incubated on ice for 30min. Cells were washed with 500µL FACS buffer, resuspended with 100µL FACS buffer +2.5µL pSTAT5(Y694)-PE (Biolegend cat#:936903), and incubated for 1 hour at RT in the dark. Cells were washed with 500µL FACS buffer and resuspended in 200µL PBS/2% PFA and kept in the dark prior to analysis on a BD LSR Fortessa X20 flow cytometer with FACSDiva software (Becton Dickinson, Mountain View CA). Data was analyzed using FlowJo (TreeStar, Inc., Ashland, OR).

To analyze reactivated cells, cells were stained for CD4, viability, and intracellular p24-Gag as previously described (54).

SEAP and Cytotoxicity Assays

HEK-Blue IL-2/15 cells, HEK-Blue IFN-α/β cells and HEK-Blue IFN-γ cells were purchased from Invivogen. Cells were maintained in Dulbecco modified Eagle medium (DMEM) supplemented with 10% (v/v) heat inactivated FBS, 1% penicillin, and 1% streptomycin (complete DMEM). Cells were selected with complete DMEM + 30µg/mL blasticidin, and 100µg/mL Zeocin. Cells were maintained in complete DMEM with 1x HEK-Blue CLR selection cocktail, and 1 µg/mL puromycin.

To evaluate the ability of HODHBt to enhance transcriptional activity of STAT1 and STAT2, HEK-Blue IFN-α/β cells and HEK-Blue IFN-γ cells were plated at 50,000 cells/well in a 96-well flat bottom plate for 24 hr prior to treatment to facilitate adherence. Cells were treated in sextuplet for each HODHBt and interferon concentration for 24 hours. After 24 hours of

544 treatment, plates were spun down at 15,000 x g for 5 minutes before 20µL of each well was
545 transferred to a fresh 96-well flat-bottom plate. Then, 180µL of prepared fresh Quanti-Blue
546 solution was added to each well and plates were incubated at 37°C for 2 hours. SEAP levels
547 were measured using a spectrophotometer at 640nm. For toxicity evaluation, 50µL of each well
548 was transferred to a fresh 96-well flat-bottom plate. Next, 50µL of prepared CytoTox 96 reagent
549 was added to each well, and the plates were incubated at room temperature in the dark for 30
550 minutes. Finally, 50µL of stop solution was added to each well and the absorbance was measured
551 using a spectrophotometer at 490nm.
552 To evaluate the transcriptional activity of AC-484 and HODHBt, HEK-Blue IL-2/15 cells
553 were used following the same protocol as detailed above. Cells were treated in sextuplet for each
554 compound and IL-15 concentration for 24 hours.
555 Western blotting
556 K562 cells were treated with the indicated conditions for 24 hours. Primary total CD4 T cells
557 were isolated from PBMCs by negative selection and treated with indicated conditions for 24
558 hours. Cells were then washed with PBS and lysed with NETN extract buffer comprised of
559 100mM NaCl, 20mM Tris-Cl (pH 8), 0.5mM EDTA, 0.5% Nonidet P-40, protease inhibitor
560 cocktail (cOmplete, Roche), and phosphatase inhibitor cocktail (phosSTOP, Roche) for 30
561 minutes on ice. Lysates were purified by centrifugation at 12,000 rpm for 10 minutes at 4°C and
562 proteins were visualized on SDS-PAGE. All primary antibodies used at 1:1000 concentrations
563 except for β-actin (1:10,000). Secondary anti-rabbit and anti-mouse antibodies were used at a
564 1:10,000 dilution.
565 Primary Cell pSTAT2 Assay

566 Naïve CD4 T cells were isolated from PBMCs from HIV-negative donors by negative selection
567 (Stemcell #19555) and activated at $0.5x10^6$ cells/mL with αCD3/CD28 Dynabeads (1:1 bead-to-
568 cell ratio) in the presence of 1μg/mL αIL-4, 2μg/mL αIL-12, and 10ng/mL for 72 hours. Cells
569 were expanded in the presence of 30IU/mL IL-2 for 48 additional hours before being treated
570 with 100μM HODHBt, 10ng/mL IFN-α, or HODHBt + IFN-α for 24 hours. pSTAT2 levels
571 were measured by flow cytometry (Cell Signaling Technologies 1° antibody).

572 Primary Cell pSTAT5 time course

573 Total CD4+ T cells were isolated via negative isolation from PBMCs from HIV negative donors.
574 Cells were then pre-treated with 100μM HODHBt, 10μM AC-484, and 5μM AC-484 for 2 hours
575 prior to the addition of 30IU/mL IL-2. The 1-hour timepoint sample was taken and stained for
576 pSTAT5 1 hour after the addition of IL-2. The 24-hour and 48-hour timepoints were stained at
577 the respective time post-IL-2 addition. For the IL-15 samples, cells were pre-treated with 100μM
578 HODHBt or10μM AC-484 for 2 hours prior to the addition of 100ng/mL IL-15. Samples were
579 stained for pSTAT5 48 hours after the addition of IL-15 and flow cytometry analysis was
580 performed as described above.

581 PBMC Immune Activation and Cytokine Analysis

582 PBMCs from HIV-negative donors were pre-treated at $3x10^6$/mL for 2 hours with 100μM
583 HODHBt, 10μM AC-484, 1μM AC-484, and 500nM AC-484; then IL-15 was added at 1ng/mL
584 and incubated for 48 hours. Cells were collected and stained for flow cytometry analysis and
585 supernatants were frozen at -20°C.

586 Frozen supernatants were thawed, and assay was performed according to manufacturer
587 protocol. Ten cytokines were measured using Quanterix SP-X Corplex Cytokine Panel (IFN-γ, IL-
588 1β, IL-4, IL-5, IL-6, IL-8, IL-10, IL-12P70, IL-22, TNFα).

589 Statistics

590 Statistical analyses were performed using GraphPad Prism 9.0 software. The statistical analysis
591 used is indicated in each figure legend.

592 Study approval

593 Volunteers 17 years and older at the Gulf Coast Regional Blood Center served as blood
594 participants. White blood cell concentrates (buffy coat) prepared from a single unit of whole
595 blood by centrifugation were purchased.

596 Data availability

597 Values for data points shown in graphs are provided in the Supporting data values file. All
598 additional data is provided in the supplemental files.

599

600 **References and Notes**

601 1. Chun TW, Stuyver L, Mizell SB, Ehler LA, Mican JA, Baseler M, et al. Presence of an
602 inducible HIV-1 latent reservoir during highly active antiretroviral therapy. *Proc Natl*
603 *Acad Sci U S A.* 1997;94(24):13193-7.

604 2. Finzi D, Hermankova M, Pierson T, Carruth LM, Buck C, Chaisson RE, et al.
605 Identification of a reservoir for HIV-1 in patients on highly active antiretroviral therapy.
606 *Science.* 1997;278(5341):1295-300.

607 3. Wong JK, Hezareh M, Günthard HF, Havlir DV, Ignacio CC, Spina CA, et al. Recovery
608 of replication-competent HIV despite prolonged suppression of plasma viremia. *Science.*
609 1997;278(5341):1291-5.

610 4. Bosque A, Nilson KA, Macedo AB, Spivak AM, Archin NM, Van Wagoner RM, et al.
611 Benzotriazoles Reactivate Latent HIV-1 through Inactivation of STAT5 SUMOylation.
612 *Cell Rep.* 2017;18(5):1324-34.

5. Bosque A, and Planelles V. Induction of HIV-1 latency and reactivation in primary memory CD4+ T cells. *Blood.* 2009;113(1):58-65.
6. Sorensen ES, Macedo AB, Resop RS, Howard JN, Nell R, Sarabia I, et al. Structure-Activity Relationship Analysis of Benzotriazine Analogues as HIV-1 Latency-Reversing Agents. *Antimicrob Agents Chemother.* 2020;64(8).
7. Macedo AB, Levinger C, Nguyen BN, Richard J, Gupta M, Cruz CRY, et al. The HIV Latency Reversal Agent HODHBt Enhances NK Cell Effector and Memory-Like Functions by Increasing Interleukin-15-Mediated STAT Activation. *J Virol.* 2022;96(15):e0037222.
8. Copertino DC, Jr., Holmberg CS, Weiler J, Ward AR, Howard JN, Levinger C, et al. The latency reversing agent HODHBt synergizes with IL-15 to enhance cytotoxic function of HIV-specific CD8+ T-cells. *JCI Insight.* 2023.
9. Martinez Molina D, and Nordlund P. The Cellular Thermal Shift Assay: A Novel Biophysical Assay for In Situ Drug Target Engagement and Mechanistic Biomarker Studies. *Annu Rev Pharmacol Toxicol.* 2016;56:141-61.
10. Jafari R, Almqvist H, Axelsson H, Ignatushchenko M, Lundback T, Nordlund P, et al. The cellular thermal shift assay for evaluating drug target interactions in cells. *Nat Protoc.* 2014;9(9):2100-22.
11. Savitski MM, Reinhard FB, Franken H, Werner T, Savitski MF, Eberhard D, et al. Tracking cancer drugs in living cells by thermal profiling of the proteome. *Science.* 2014;346(6205):1255784.
12. ten Hoeve J, de Jesus Ibarra-Sanchez M, Fu Y, Zhu W, Tremblay M, David M, et al. Identification of a nuclear Stat1 protein tyrosine phosphatase. *Mol Cell Biol.* 2002;22(16):5662-8.

13. Yamamoto T, Sekine Y, Kashima K, Kubota A, Sato N, Aoki N, et al. The nuclear isoform of protein-tyrosine phosphatase TC-PTP regulates interleukin-6-mediated signaling pathway through STAT3 dephosphorylation. *Biochem Biophys Res Commun.* 2002;297(4):811-7.

14. Fukushima A, Loh K, Galic S, Fam B, Shields B, Wiede F, et al. T-cell protein tyrosine phosphatase attenuates STAT3 and insulin signaling in the liver to regulate gluconeogenesis. *Diabetes.* 2010;59(8):1906-14.

15. Tiganis T. PTP1B and TCPTP--nonredundant phosphatases in insulin signaling and glucose homeostasis. *FEBS J.* 2013;280(2):445-58.

16. Baumgartner CK, Ebrahimi-Nik H, Iracheta-Vellve A, Hamel KM, Olander KE, Davis TGR, et al. The PTPN2/PTPN1 inhibitor ABBV-CLS-484 unleashes potent anti-tumour immunity. *Nature.* 2023;622(7984):850-62.

17. Klein E, Ben-Bassat H, Neumann H, Ralph P, Zeuthen J, Polliack A, et al. Properties of the K562 cell line, derived from a patient with chronic myeloid leukemia. *Int J Cancer.* 1976;18(4):421-31.

18. de Groot RP, Raaijmakers JA, Lammers JW, Jove R, and Koenderman L. STAT5 activation by BCR-Abl contributes to transformation of K562 leukemia cells. *Blood.* 1999;94(3):1108-12.

19. Frangioni JV, Beahm PH, Shifrin V, Jost CA, and Neel BG. The nontransmembrane tyrosine phosphatase PTP-1B localizes to the endoplasmic reticulum via its 35 amino acid C-terminal sequence. *Cell.* 1992;68(3):545-60.

20. Lorenzen JA, Dadabay CY, and Fischer EH. COOH-terminal sequence motifs target the T cell protein tyrosine phosphatase to the ER and nucleus. *J Cell Biol.* 1995;131(3):631-43.

21. Ota J, Kimura F, Sato K, Wakimoto N, Nakamura Y, Nagata N, et al. Association of CrkL with STAT5 in hematopoietic cells stimulated by granulocyte-macrophage colony-stimulating factor or erythropoietin. *Biochem Biophys Res Commun.* 1998;252(3):779-86.

22. Wiede F, Lu KH, Du X, Zeissig MN, Xu R, Goh PK, et al. PTP1B Is an Intracellular Checkpoint that Limits T-cell and CAR T-cell Antitumor Immunity. *Cancer Discov.* 2022;12(3):752-73.

23. Wiede F, Lu KH, Du X, Liang S, Hochheiser K, Dodd GT, et al. PTPN2 phosphatase deletion in T cells promotes anti-tumour immunity and CAR T-cell efficacy in solid tumours. *EMBO J.* 2020;39(2):e103637.

24. Tautz L, Critton DA, and Grotegut S. Protein tyrosine phosphatases: structure, function, and implication in human disease. *Methods Mol Biol.* 2013;1053:179-221.

25. Bourdeau A, Dube N, and Tremblay ML. Cytoplasmic protein tyrosine phosphatases, regulation and function: the roles of PTP1B and TC-PTP. *Curr Opin Cell Biol.* 2005;17(2):203-9.

26. Nelson DL. *Lehninger principles of biochemistry.* Fourth edition. New York : W.H. Freeman, 2005.; 2005.

27. Ramsay RR, and Tipton KF. Assessment of Enzyme Inhibition: A Review with Examples from the Development of Monoamine Oxidase and Cholinesterase Inhibitory Drugs. *Molecules.* 2017;22(7).

28. Ivashkiv LB, and Hu X. Signaling by STATs. *Arthritis Res Ther.* 2004;6(4):159-68.

29. Darnell JE, Jr. STATs and gene regulation. *Science.* 1997;277(5332):1630-5.

30. Nelson N, Marks MS, Driggers PH, and Ozato K. Interferon consensus sequence-binding protein, a member of the interferon regulatory factor family, suppresses interferon-induced gene transcription. *Mol Cell Biol.* 1993;13(1):588-99.

31. Weisz A, Kirchhoff S, and Levi BZ. IFN consensus sequence binding protein (ICSBP) is a conditional repressor of IFN inducible promoters. *Int Immunol.* 1994;6(8):1125-31.
32. Tiganis T, and Bennett AM. Protein tyrosine phosphatase function: the substrate perspective. *Biochem J.* 2007;402(1):1-15.
33. Lim CP, and Cao X. Structure, function, and regulation of STAT proteins. *Mol Biosyst.* 2006;2(11):536-50.
34. Miller JS, Davis ZB, Helgeson E, Reilly C, Thorkelson A, Anderson J, et al. Safety and virologic impact of the IL-15 superagonist N-803 in people living with HIV: a phase 1 trial. *Nat Med.* 2022;28(2):392-400.
35. Bentires-Alj M, and Neel BG. Protein-tyrosine phosphatase 1B is required for HER2/Neu-induced breast cancer. *Cancer Res.* 2007;67(6):2420-4.
36. Manguso RT, Pope HW, Zimmer MD, Brown FD, Yates KB, Miller BC, et al. In vivo CRISPR screening identifies Ptpn2 as a cancer immunotherapy target. *Nature.* 2017;547(7664):413-8.
37. Song J, Lan J, Tang J, and Luo N. PTPN2 in the Immunity and Tumor Immunotherapy: A Concise Review. *Int J Mol Sci.* 2022;23(17).
38. Flosbach M, Oberle SG, Scherer S, Zecha J, von Hoesslin M, Wiede F, et al. PTPN2 Deficiency Enhances Programmed T Cell Expansion and Survival Capacity of Activated T Cells. *Cell Rep.* 2020;32(4):107957.
39. Zhang ZY, and Lee SY. PTP1B inhibitors as potential therapeutics in the treatment of type 2 diabetes and obesity. *Expert Opin Investig Drugs.* 2003;12(2):223-33.
40. Lantz KA, Hart SG, Planey SL, Roitman MF, Ruiz-White IA, Wolfe HR, et al. Inhibition of PTP1B by trodusquemine (MSI-1436) causes fat-specific weight loss in diet-induced obese mice. *Obesity (Silver Spring).* 2010;18(8):1516-23.

41. Thareja S, Aggarwal S, Bhardwaj TR, and Kumar M. Protein tyrosine phosphatase 1B inhibitors: a molecular level legitimate approach for the management of diabetes mellitus. *Med Res Rev.* 2012;32(3):459-517.

42. Dodd GT, Xirouchaki CE, Eramo M, Mitchell CA, Andrews ZB, Henry BA, et al. Intranasal Targeting of Hypothalamic PTP1B and TCPTP Reinstates Leptin and Insulin Sensitivity and Promotes Weight Loss in Obesity. *Cell Rep.* 2019;28(11):2905-22 e5.

43. Liang S, Tran E, Du X, Dong J, Sudholz H, Chen H, et al. A small molecule inhibitor of PTP1B and PTPN2 enhances T cell anti-tumor immunity. *Nat Commun.* 2023;14(1):4524.

44. Kiernan RE, Vanhulle C, Schiltz L, Adam E, Xiao H, Maudoux F, et al. HIV-1 tat transcriptional activity is regulated by acetylation. *EMBO J.* 1999;18(21):6106-18.

45. Lusic M, Marcello A, Cereseto A, and Giacca M. Regulation of HIV-1 gene expression by histone acetylation and factor recruitment at the LTR promoter. *EMBO J.* 2003;22(24):6550-61.

46. du Chene I, Basyuk E, Lin YL, Triboulet R, Knezevich A, Chable-Bessia C, et al. Suv39H1 and HP1gamma are responsible for chromatin-mediated HIV-1 transcriptional silencing and post-integration latency. *EMBO J.* 2007;26(2):424-35.

47. Imai K, Togami H, and Okamoto T. Involvement of histone H3 lysine 9 (H3K9) methyltransferase G9a in the maintenance of HIV-1 latency and its reactivation by BIX01294. *J Biol Chem.* 2010;285(22):16538-45.

48. Kao SY, Calman AF, Luciw PA, and Peterlin BM. Anti-termination of transcription within the long terminal repeat of HIV-1 by tat gene product. *Nature.* 1987;330(6147):489-93.

49. Lassen KG, Bailey JR, and Siliciano RF. Analysis of human immunodeficiency virus type 1 transcriptional elongation in resting CD4+ T cells in vivo. *J Virol.* 2004;78(17):9105-14.

50. Karn J, and Stoltzfus CM. Transcriptional and posttranscriptional regulation of HIV-1 gene expression. *Cold Spring Harb Perspect Med.* 2012;2(2):a006916.

51. Lassen KG, Ramyar KX, Bailey JR, Zhou Y, and Siliciano RF. Nuclear retention of multiply spliced HIV-1 RNA in resting CD4+ T cells. *PLoS Pathog.* 2006;2(7):e68.

52. Mangeat B, Turelli P, Caron G, Friedli M, Perrin L, and Trono D. Broad antiretroviral defence by human APOBEC3G through lethal editing of nascent reverse transcripts. *Nature.* 2003;424(6944):99-103.

53. Yukl SA, Kaiser P, Kim P, Telwatte S, Joshi SK, Vu M, et al. HIV latency in isolated patient CD4(+) T cells may be due to blocks in HIV transcriptional elongation, completion, and splicing. *Sci Transl Med.* 2018;10(430).

54. Martins LJ, Bonczkowski P, Spivak AM, De Spiegelaere W, Novis CL, DePaula-Silva AB, et al. Modeling HIV-1 Latency in Primary T Cells Using a Replication-Competent Virus. *AIDS Res Hum Retroviruses.* 2016;32(2):187-93.

55. Sarabia I, Huang SH, Ward AR, Jones RB, and Bosque A. The Intact Non-Inducible Latent HIV-1 Reservoir is Established In an In Vitro Primary T(CM) Cell Model of Latency. *J Virol.* 2021;95(7).

Acknowledgments: We would like to thank Xabier Arias-Moreno for his insightful comments while preparing this manuscript. Additionally, we would like to thank Heidi Schubert for her consultation and expert advice while preparing this manuscript.

Funding:

National Institutes of Health grant R21/R33 AI116212 (AB)

National Institutes of Health grant R56 AI145683 (AB)

This research has been facilitated by the services and resources provided by District of Columbia, Center for AIDS research, an NIH funded program (AI117970), which is supported by the following NIH co-funding and participating institutes and centers: NIAID, NCI, NICJD, NHLBI, NIDA, NINH, NIA, FIC, NIGGIS and NDDK and OAR. The content is solely the responsibility of the authors and does not necessarily represent the official views of the NIH.

Author contributions:

AB, JNH conceptualized the work. JNH, TDZ, CL, MS, DCC, and AB designed methodology and experiments were carried out by JNH, TDZ, WW, DCC, MS, CL, ER, and EKM. AB acquired funding and performed project administration. AB, RBJ, and NSS supervised experimental output and manuscript preparation. JNH and AB wrote original manuscript and JNH, NSS, TDZ, and AB reviewed and edited the final manuscript.

Competing interests: AB has a patent application on the use of HODHBt and other benzotriazine derivatives to enhance immune responses and patent on the use of HODHBt and other benzotriazine derivatives as latency reversing agents. The rest of the authors declare no conflict of interest.

Supplementary Materials

Supplemental Figures 1-7

Supplementary Files 1-3

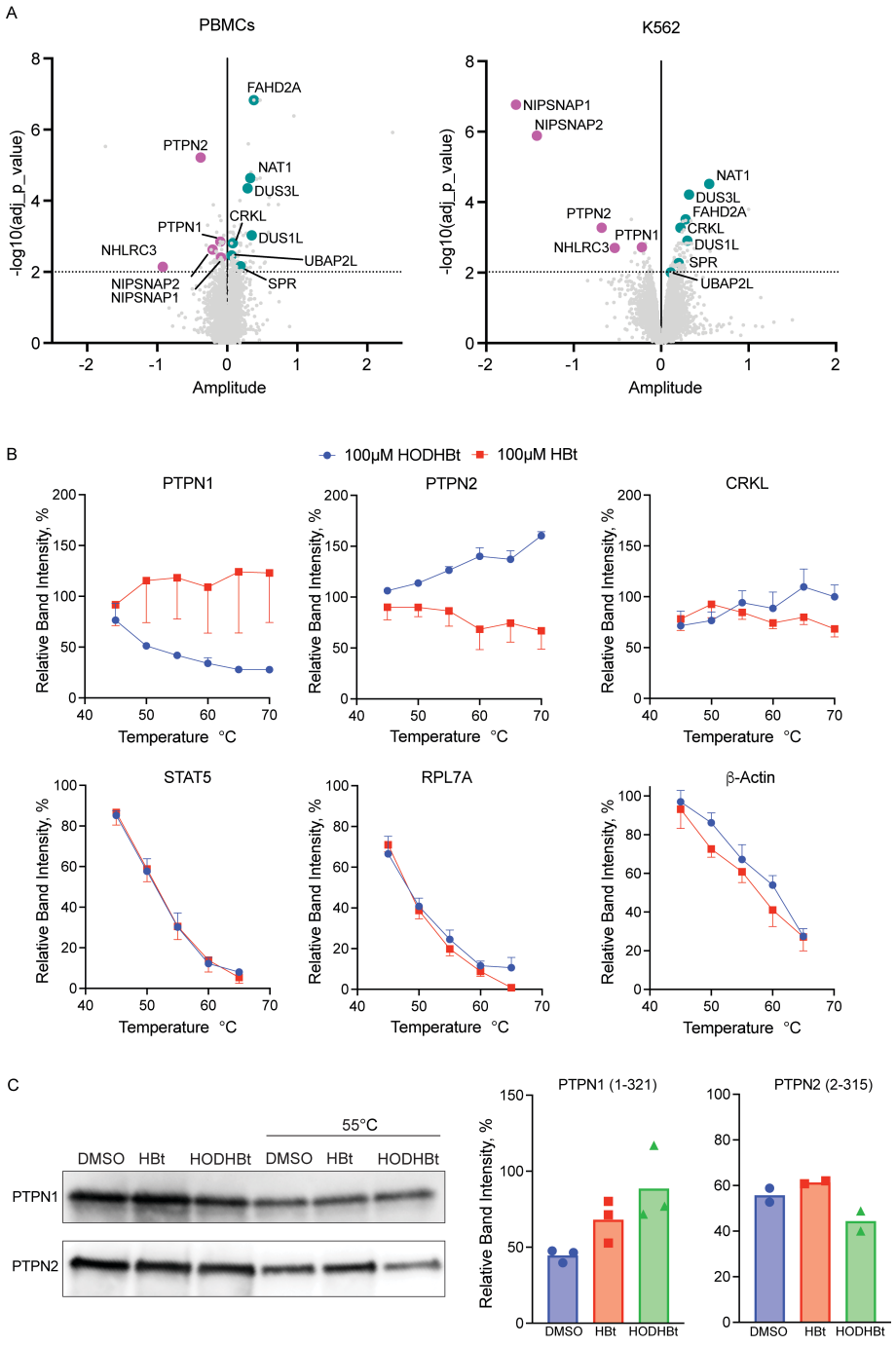

Figure 1. HODHBt modulates the thermal stability of PTPN1 and PTPN2 in vitro

(**A**) Compressed CETSA-MS results indicating changes in thermal stability of protein in both PBMCs and K562. X-axis represents amplitude (log_2 fold-change), and y-axis represents effect significance ($-log_{10}$(p-value)). Statistically significant ($p<0.01$) proteins in common between PBMCs and K562 cells are indicated. (**B**) Thermal melting curves for PTPN1, PTPN2, CRKL, STAT5, RPL7A and β-actin in CD4 T cell lysates after treatment with 100μM HODHBt vs 100μM HBt (n=2-4). (**C**) Purified PTPN1 catalytic domain and purified commercial PTPN2 catalytic domain CETSA after treatment with DMSO, 100μM HODHBt, or 100μM HBt (n=2-3).

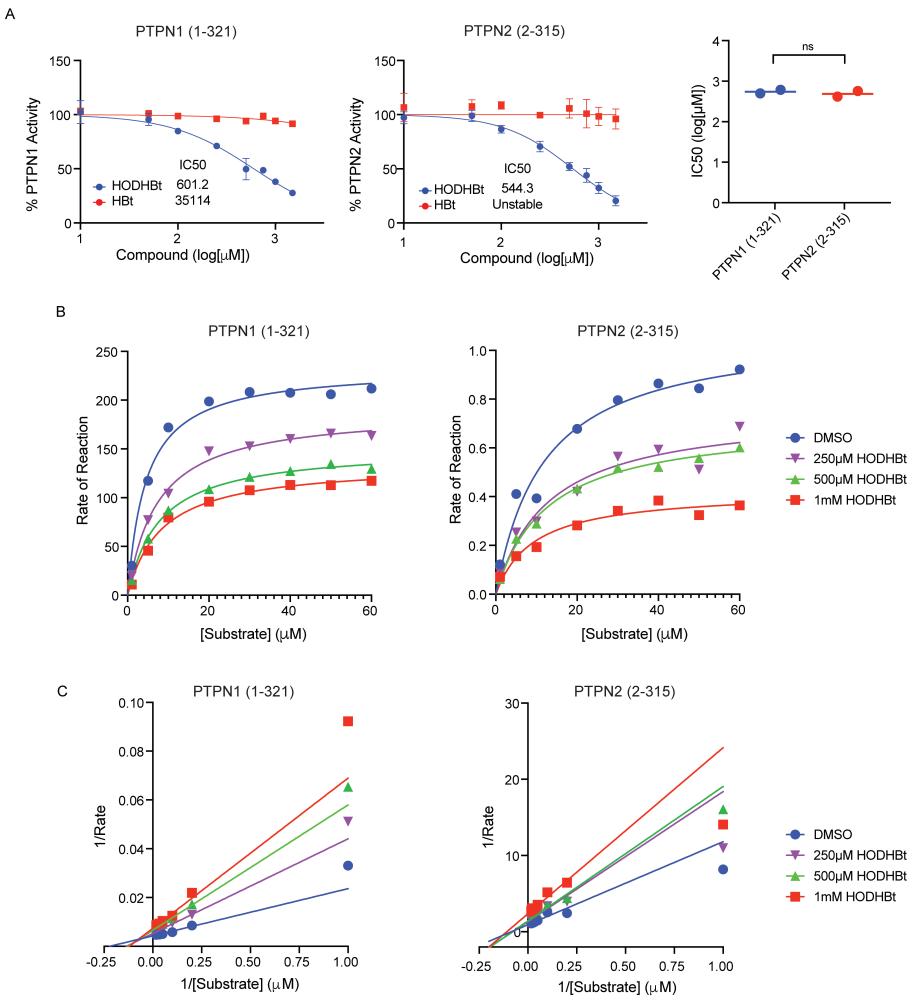

Figure 2. HODHBt is a mixed inhibitor of PTPN1 and PTPN2

(**A**) HODHBt directly inhibits the catalytic activity of the catalytic domain of PTPN1and the catalytic domain of PTPN2 using a fluorogenic assay (n=2). Error bars indicate SD. IC_{50} values calculated for 2 independent experiments. (**B**) Effect of HODHBt on PTPN1- and PTPN2-catalyzed fluorogenic PTPN1 substrate. (**C**) Lineweaver-Burk plots.

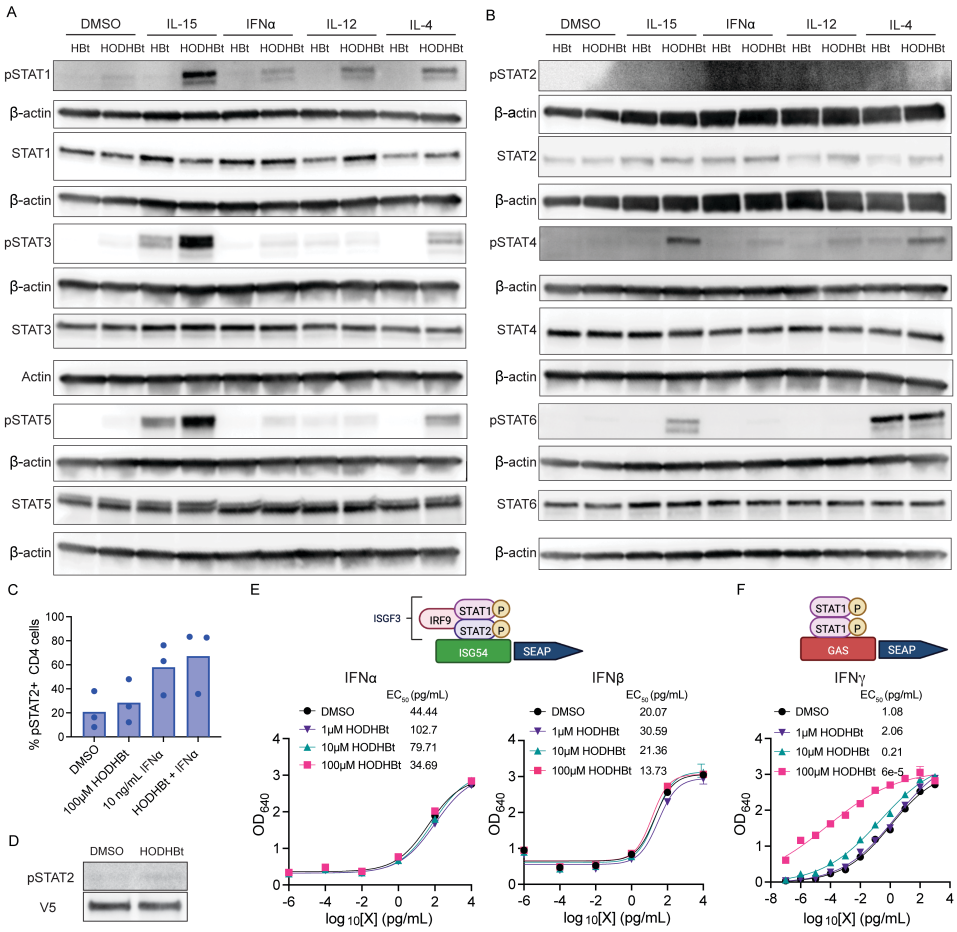

Figure 3. Inhibiting PTPN1 and PTPN2 with HODHBt enhances activation of different STATs in a cytokine-dependent manner.

Analysis of phosphorylation levels of STAT-1, 3, and 5 (**A**) or STAT-2, 4, and 6 (**B**) in primary total CD4 T cells after treatment with DMSO, 100ng/mL IL-15, 1ng/mL IFN-α, 2ng/mL IL-12, and 2ng/mL IL-4 in the presence of 100μM HODHBt or HBt for 24 hours. (**C**) Levels of pSTAT2+ cells in naïve CD4 T cells treated with 100μM HODHBt +/- 10 ng/mL IFN-α for 24 hours (n=3). (**D**) Levels of STAT2 phosphorylation after transfection of V5-STAT2 into 293FT cells and treatment with DMSO or 100μM HODHBt. (**E**) Dose response of STAT1/2 transcriptional activity mediated by IFN-α (left) and IFN-β (right) in the presence of 1, 10, or 100μM HODHBt in HEK-Blue IFNα/β cells. The data represent the mean ± the SD of an experiment performed in triplicate. (**F**) Dose response of STAT1 transcriptional activity mediated by IFN-γ in the presence of 1, 10, or 100μM HODHBt in HEK-Blue IFNγ cells. The data represent the mean ± the SD of an experiment performed in triplicate.

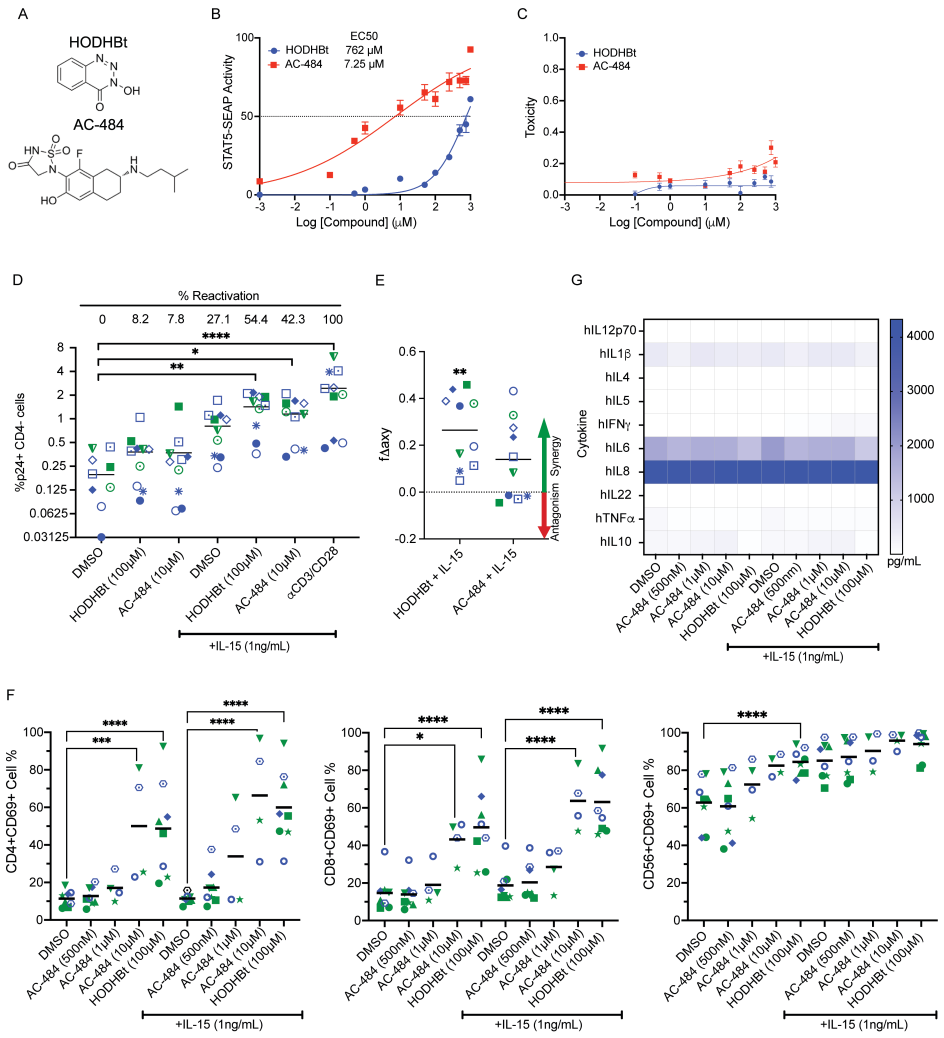

Figure 4. AC-484 promotes immune activation and synergizes with IL-15 to reactivate latent HIV.

(**A**) Structure comparison of HODHBt and AC-484. Measurement of STAT5 transcriptional activity (**B**) and toxicity (**C**) after treatment with dose response of HODHBt and AC-484 in HEK-Blue- IL2/IL15 cells. The data represent the mean ± the SD of an experiment performed in duplicate. (**D**) Reactivation of latent HIV in T_{CM} measured by flow cytometry after treatment with 100μM HODHBt or 10μM AC-484 +/- 100ng/mL IL-15, or αCD3/CD28 (n=10). Dunnett's multiple comparisons test was used to calculate p-values (*p < 0.05; **p<0.01; ****p<0.0001). (**E**) Bliss independence synergy calculations for reactivation. Wilcoxon matched-pairs signed rank test was used to calculate p values (*p < 0.05; **p < 0.01). (**F**) PBMCs were treated with 100μM HODHBt and a dose response of AC-484 +/- 1ng/mL IL-15 for 48 hours and CD69 induction was analyzed by flow cytometry in CD4 T cells, CD8 T cells, and NK cells (n=4-8). Data are the average effect from 4-8 donors. Tukey's multiple comparisons test was used to calculate p values (*p < 0.05; ***p<0.001; ****p<0.0001). (**G**) Secretion of pro- and anti-inflammatory cytokine were measured using a 10-plex cytokine ELISA in supernatants from (**F**).

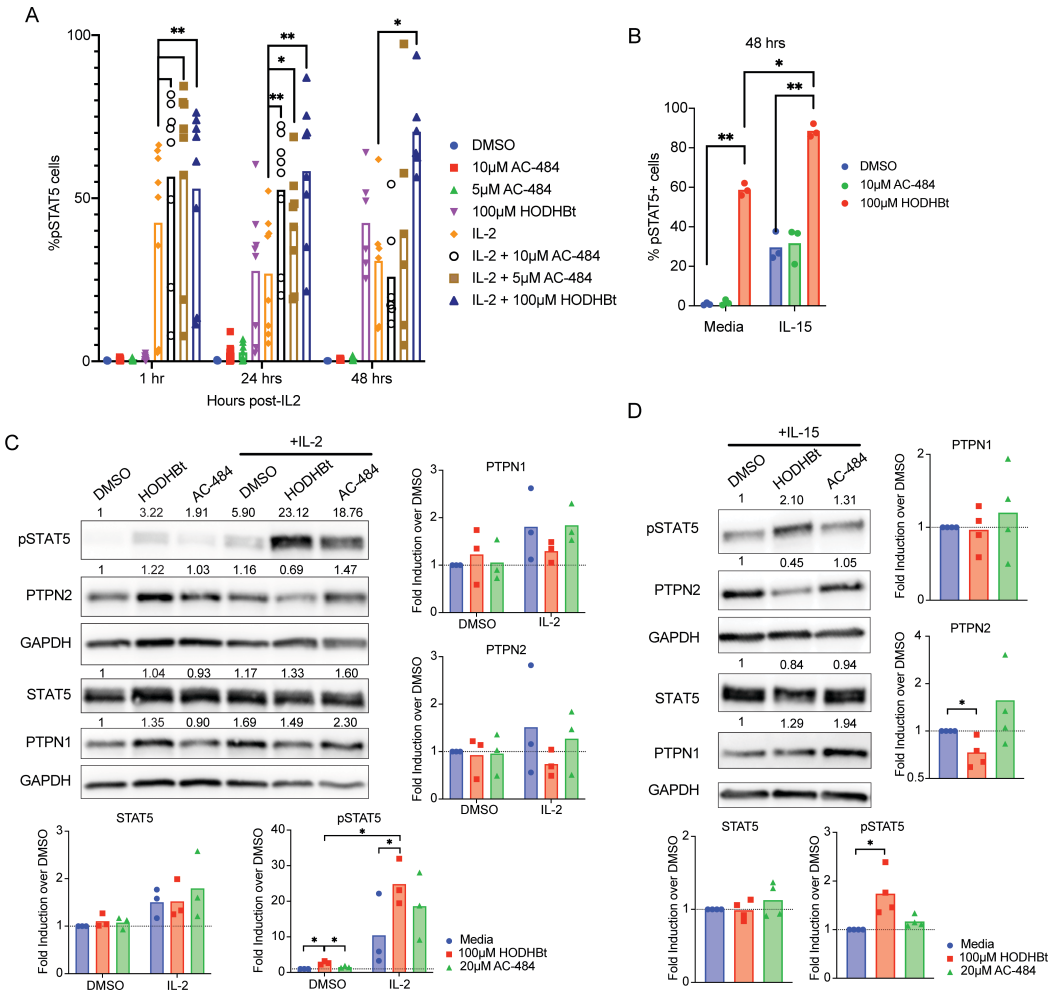

Figure 5. HODHBt and AC-484 have differing effects on STAT5 phosphorylation.
(**A**) Total CD4s were pre-treated with 100μM HODHBt, 10μM AC-484, and 5μM AC-484 for 2 hours prior to the addition of IL-2. pSTAT5 levels were measured by flow cytometry 1hr, 24h and 48h after stimulation with IL-2 (n=6). Wilcoxon matched-pairs signed rank test was used to calculate p values (*$p < 0.05$; **$p < 0.01$). (**B**) Total CD4s were pre-treated with 100μM HODHBt or 10μM AC-484 for 2 hours prior to the addition of IL-15. pSTAT5 levels were measured by flow cytometry 48h after stimulation with IL-2 (n=3). Paired t-test was used to calculate p values (*$p < 0.05$; **$p < 0.01$). Protein levels of PTPN1, PTPN2, pSTAT5, and STAT5 were measured by western blot in CD4s pre-treated with 100μM HODHBt or 20μM AC-484 for 2 hours before the addition of IL-2 (**C**) and IL-15 (**D**) for 24 hours (n=3). Paired t-test was used to calculate p values (*$p < 0.05$).

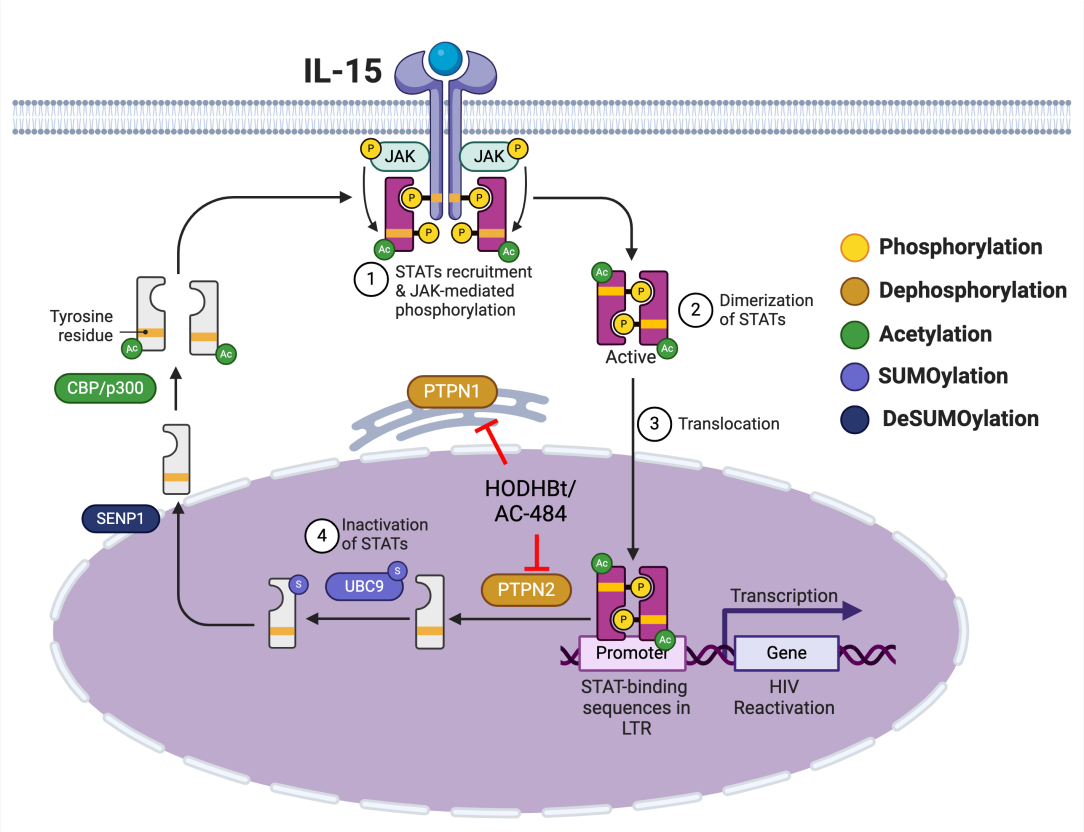

Figure 6. Proposed mechanism of action of HODHBt and AC-484. Created with Biorender.com